APPROXIMATION FOR DISTRIBUTION OF FLOW PROPERTIES IN THE ANGLE-OF-ATTACK PLANE OF CONICAL FLOWS

by Joseph W. Cleary

Ames Research Center
Moffett Field, Calif. 94035

NATIONAL AERONAUTICS AND SPACE ADMINISTRATION • WASHINGTON, D. C. • AUGUST 1970

1. Report No.	2. Government Accession No.	3. Recipient's Catalog No.
NASA TN D-5951		

4. Title and Subtitle
APPROXIMATION FOR DISTRIBUTION OF FLOW PROPERTIES IN THE ANGLE-OF-ATTACK PLANE OF CONICAL FLOWS

5. Report Date
August 1970

6. Performing Organization Code

7. Author(s)
Joseph W. Cleary

8. Performing Organization Report No.
A-3615

9. Performing Organization Name and Address
NASA Ames Research Center
Moffett Field, California 94035

10. Work Unit No.
129-01-03-10-00-21

11. Contract or Grant No.

12. Sponsoring Agency Name and Address
National Aeronautics and Space Administration
Washington, D. C., 20546

13. Type of Report and Period Covered
Technical Note

14. Sponsoring Agency Code

15. Supplementary Notes

16. Abstract

A simple approximation is made for the hodographs of stagnation-line streamlines in the angle-of-attack plane of conical flows that yields explicit equations for distributions of velocity and flow angle. It is assumed that shock angle and surface inclination are known and the flow is inviscid and isentropic. Comparisons with exact numerical solutions of the flow over right-circular cones demonstrate agreement over a wide range of cone angles and angles of attack for Mach numbers from one to infinity.

17. Key Words (Suggested by Author(s))
Conical flow
Angle-of-attack plane
Inviscid approximation
Distributions of velocity
Distributions of flow angle
Stagnation line

18. Distribution Statement
Unclassified - Unlimited

19. Security Classif. (of this report)	20. Security Classif. (of this page)	21. No. of Pages	22. Price*
Unclassified	Unclassified	22	$3.00

*For sale by the Clearinghouse for Federal Scientific and Technical Information
Springfield, Virginia 22151

NOTATION

a	major axis
b	minor axis
c	speed of sound
B	a parameter (eq. (8))
f, F	functions of ω_c (eqs. (B2) and (B3), respectively)
$\bar{H}$, $\bar{K}$	coordinates of the center of a circular-arc (eqs. (3) and (4), respectively)
M	Mach number
p	pressure
$\bar{Q}$	dimensionless quantity (eq. (16))
R	radius of curvature
$\bar{R}$	effective radius of curvature (eq. (2))
T	temperature
u, v	components of V
V	velocity
V_m	maximum speed obtainable by expanding to zero absolute temperature
x	body reference axis
α	angle of attack
γ	ratio of specific heats
δ	semiapex angle
ϵ	incremental velocity component
θ	conical coordinate measured from free-stream direction
ν	angle between body reference axis and entropy singular line

ρ	density
ω	angle of the flow to free-stream direction

Subscripts

2	immediately behind shock
c	cone surface
e	exact value
E	effective value
s	swept-cylinder stagnation line
∞	free stream
n	normal component to shock
max	maximum value
t	total value

APPROXIMATION FOR DISTRIBUTION OF FLOW PROPERTIES IN THE ANGLE-OF-ATTACK PLANE OF CONICAL FLOWS

Joseph W. Cleary

Ames Research Center

SUMMARY

An approximation is made for the hodographs of stagnation-line streamlines in the angle-of-attack plane of conical flows that yields explicit equations for distributions of velocity and flow angle. It is assumed that shock angle and surface inclination are known and the flow is inviscid and isentropic. In essence, the approximation replaces streamline hodographs of conical flows by circular arcs. Streamline hodographs of wedge and swept-cylinder flows are obtained from the solution as special limiting cases of conical flow. The approximation introduces no limitation on angle of attack or body shape as long as shocks are straight and flows are conical.

Comparisons of the approximation with exact numerical solutions for the flow over right-circular cones demonstrate agreement for Mach numbers from one to infinity over a wide range of cone angles and angles of attack. Comparisons with experimental results show applicability of the approximation to conical flows other than those for right-circular cones.

INTRODUCTION

Theoretical aspects of conical flows are of fundamental interest to aerodynamic research and to the more practical problems of vehicle design. The direct application to lifting entry configurations has enlivened interest in conical-flow theory for a wide range of angles of attack and body shapes. The flow in the angle-of-attack plane is of unique interest in conical flow applications since flap-type controls may be placed on the windward stagnation line in order to achieve greater effectiveness from compression of the flow. Moreover, heating is apt to be most severe on the windward stagnation line.

Knowledge of the compression process in the angle-of-attack plane is required to adequately estimate control effectiveness and heating. Although inviscid axisymmetric solutions by numerical methods are available (e.g., refs. 1 to 3) for estimating the compression process at 0° angle of attack, only limited solutions have been published for estimating the compression of the flow at angle of attack (refs. 4 and 5). Moreover, at present, numerical solutions of the flow generally require that three-dimensional bodies be smooth without sharp edges. Since conical-type bodies with sharp edges on the windward surface may prove useful for achieving high drag at high angles

of attack during entry, some method is needed for calculating the compression process of conical flows in general.

The purpose of the present study is to present an approximate solution for the compression process of the flow in the angle-of-attack plane. A semiempirical approach is used to develop closed-form equations for the distribution of flow properties between the shock and the body in this plane. While it is assumed that surface inclination and shock angle are known, no limitation is made on angle of attack or body shape to the extent that shock-wave elements are straight and the flow is conical. Comparisons are made with numerical solutions and with experiment to demonstrate accuracy and general applicability.

ANALYSIS

Description of the Approximation and Presentation of Equations

The intent of the present analysis is to develop an approximation for the distribution of properties of the flow in the angle-of-attack plane of conical flows. It is assumed at the outset that the shock angle θ_2 and surface inclination ω_c are known and that, as depicted in figure 1, the flow between the shock and the body in the angle-of-attack plane is inviscid and isentropic. Before the approximation is described, the true relationship between velocity vectors and angles pertinent to conical flows will be examined. This relationship can be shown most clearly by a plot of the velocity component v as a function of u (hodograph coordinates). Such a plot can also be considered a polar diagram with radius vector V given as a function of the turning angle of the flow ω. It is expedient to consider the hodographs of axisymmetric flows first and then consideration will be given to other conical flows.

Axisymmetric conical flows- Figure 2 shows the hodograph of a streamline of a typical axisymmetric conical flow. In figure 2, R is the local radius of curvature of the streamline hodograph at an arbitrary point p in the conical field. Note that since R is normal to the streamline hodograph, an extension of R makes the conical coordinate angle θ with the free-stream direction. Furthermore, points 2 and c correspond to conditions at the shock and cone surface, respectively; points 2', p', and c' represent end points of R that correspond with points 2, p, and c, respectively. In the present case the magnitude of R was evaluated by an exact equation given by Busemann (refs. 6 and 7). Busemann's equation was used to determine R and the locus of end points of R from an exact numerical solution of the flow. While the differential equation of the streamline hodograph is known (ref. 7), no general solutions are known. Therefore, an approximation is considered appropriate.

In essence, the present approximation replaces the exact hodograph by a circular arc. Details of the procedure are shown in figure 3 where R is

replaced by a constant effective radius of curvature $\bar{R}$ whose center is at $\bar{H}$ and $\bar{K}$. The circular arc passes through point 2 and has its center at the intersection of R_2 and R_c (or an extension of V_c). Since R and $\bar{R}$ are both normal to the streamline hodograph at point 2, the exact velocity and slope dv/du are retained in the approximation at the shock wave. While the exact value of dv/du at the cone surface is also retained, the surface velocity is in error by an unknown amount.

The circular-arc approximation is given by equation (1).

$$(u - \bar{H})^2 + (v - \bar{K})^2 = \bar{R}^2 \tag{1}$$

Equations for $\bar{R}$, $\bar{H}$, and $\bar{K}$ are derived in appendix A and are given by (2), (3), and (4), respectively:

$$\bar{R} = V_\infty \frac{\sin(\omega_c - \omega_2)\cos\theta_2}{\sin(\theta_2 - \omega_c)\cos(\theta_2 - \omega_2)} \tag{2}$$

$$\bar{H} = V_\infty \frac{\tan(\theta_2 - \omega_2)}{\sin(\theta_2 - \omega_c)} \cos\theta_2 \cos\omega_c \tag{3}$$

$$\bar{K} = V_\infty \frac{\tan(\theta_2 - \omega_2)}{\sin(\theta_2 - \omega_c)} \cos\theta_2 \sin\omega_c \tag{4}$$

where θ_2, ω_2, and $\omega_c = \delta_c$ are known quantities. Furthermore, it is shown in appendix A that by substitution of $u = V\cos\omega$ and $v = V\sin\omega$ and the known values of $\bar{R}$, $\bar{H}$, and $\bar{K}$ in equation (1), V/V_∞ is given as a function of $(\omega_c - \omega)$ by equation (5).

$$\frac{V}{V_\infty} = \frac{\cos\theta_2 \tan(\theta_2 - \omega_2)}{\sin(\theta_2 - \omega_c)} \left\{ \cos(\omega_c - \omega) - \left[\cos^2(\omega_c - \omega) - 1 + \frac{\sin^2(\omega_c - \omega_2)}{\sin^2(\theta_2 - \omega_2)} \right]^{1/2} \right\} \tag{5}$$

Since additional pertinent equations are derived in appendix A, it is sufficient here to summarize the final results.

Velocity distributions normalized by V_∞ and V_c are given as functions of the conical coordinate $(\theta - \omega_c)$ by equations (6) and (7), respectively,

$$\frac{V}{V_\infty} = \cos\theta_2 \left[\frac{\rho_\infty}{\rho_2}\tan\theta_2 \tan\frac{1}{2}(\theta_2-\omega_c)+1\right]\left\{1+\frac{2B}{(1-B)^2}[1-\cos(\theta-\omega_c)]\right\}^{1/2} \tag{6}$$

$$\frac{V}{V_c} = \left\{1+\frac{2B}{(1-B)^2}[1-\cos(\theta-\omega_c)]\right\}^{1/2} \tag{7}$$

where the parameter B is given by equation (8)

$$B = \cos(\theta_2 - \omega_c) - \frac{\sin(\theta_2 - \omega_c)}{(\rho_\infty/\rho_2)\tan\theta_2} \tag{8}$$

and the density ratio across the shock ρ_∞/ρ_2 by equation (9) (see ref. 8)

$$\frac{\rho_\infty}{\rho_2} = \frac{2}{\gamma+1}\left(\frac{1}{M_{\infty_n}^2} + \frac{\gamma-1}{2}\right) \tag{9}$$

Properties of the flow at the cone surface are of particular interest and can be evaluated from equation (6) by specifying that $\theta = \omega_c$ to give equation (10)

$$\frac{V_c}{V_\infty} = \cos\theta_2\left[\frac{\rho_\infty}{\rho_2}\tan\theta_2\tan\frac{1}{2}(\theta_2-\omega_c)+1\right] \tag{10}$$

The local flow angle $(\omega_c - \omega)$ is given by equation (11) as a function of the conical coordinate $(\theta - \omega_c)$.

$$\omega_c - \omega = \tan^{-1}\left[\frac{B\sin(\theta-\omega_c)}{1-B\cos(\theta-\omega_c)}\right] \tag{11}$$

An interpretation of how to apply equations (1) to (11) to conical flows in general will now be given.

Other conical flows- Since in the angle-of-attack plane conical flow is characteristically isentropic, there is a close relationship between the axisymmetric solution and conical flows in general. Therefore, it is assumed in like manner that a circular arc approximates the streamline hodograph of

the general conical flow. Within this assumption equations (1) to (11) are applied to the general case $\alpha > 0^\circ$ by assigning $\omega_c = \delta_c + \alpha$ and $\omega_c = \delta_c - \alpha$ on the windward and leeward stagnation lines, respectively. If on the leeward side the singular line, for which entropy is multivalued, has lifted from the surface, then $\omega_c = \nu - \alpha$ where ν is the angle between the cone reference axis and the singular line.

The usefulness of the circular-arc assumption for $\alpha > 0^\circ$ will be scrutinized later when the approximation is compared with exact numerical solutions. At present, support for it can be given by examining two limiting conical flows in the hodograph plane; these are the flow over a wedge and the flow in the sweep plane of swept cylinders. Figure 4 shows the hodographs of these flows and of their streamlines together with that of a typical conical flow. The hodograph for wedge flows is, of course, the shock polar while that for swept cylinder flows is the trace of the component of velocity parallel to the wave and is given by the semicircle $V_s/V_\infty = \cos \theta_2$.

For a specified θ_2, the streamline hodograph for wedge flow is point 2 (u and v constant) on the shock polar; that for the swept cylinder is a straight-line extension of the change in velocity through the shock wave from point 2 to point s on the swept-cylinder polar (see fig. 4). Results from a limited number of exact numerical solutions for conical flows (refs. 1 to 5) demonstrate that V_c must terminate within the region bounded by the shock and swept-cylinder polars and therefore, this is accepted as a factual condition. Moreover, numerical solutions show that for a specified θ_2 and ω, the velocity of conical flow exceeds that for a swept cylinder, but this velocity is, of course, less than that for a wedge having the same θ_2. Therefore, it can be shown that the inequality given by (12) applies (see fig. 4).

$$V_s < V_\infty \frac{\cos \theta_2}{\cos(\theta_2 - \omega_c)} < V_c < V < V_2 \tag{12}$$

For constant θ_2 it is apparent that there is a spectrum of conical flows whose limits are the flow over a wedge and a swept cylinder. For these flows equation (10) predicts a single distribution of V_c/V_∞ as a function of ω_c. Wedge and swept-cylinder flows are limiting cases for which $\omega_c = \omega_2$ and $\omega_c = \theta_2$, respectively, as can be verified by substitution in equation (10) to yield the respective exact results $V_c/V_\infty = V_2/V_\infty = \cos \theta_2/\cos(\theta_2 - \omega_2)$ and $V_c/V_\infty = V_s/V_\infty = \cos \theta_2$. Similarly, as demonstrated in appendix B, it can be shown that distributions of V/V_∞ given by equation (5) contain wedge and swept-cylinder distributions as special cases.

Finally, consider the effects of M_∞ and γ on the present approximation. As M_∞ increases or γ decreases, the shock polar grows in size and in the limit $M_\infty = \infty$ and $\gamma = 1$ coincides with the swept-cylinder polar. It is evident that for this limit, $\omega_c = \omega_2 = \theta_2$ and $V_c = V_s = V_2 = V_\infty \cos \theta_2$.

Furthermore, as the limit is approached the length of the streamline hodograph of V is shortened and $V_c \rightarrow V_2$. Consequently, the accuracy of the approximation is improved, as will be demonstrated later by comparisons with exact numerical solutions. First, however, before demonstrating accuracy, equations will be given for other flow properties in a form to expedite estimates.

Equations of state properties- Since the flow in the angle-of-attack plane is isentropic, other flow properties can be estimated locally by use of equation (6) in conjunction with Bernoulli's equation and equations from supersonic flow and oblique-shock theories. Equations for other flow properties were derived from equations given in reference 8 and are summarized below for completeness.

$$\frac{T}{T_\infty} = \frac{\frac{\gamma + 1}{\gamma - 1}\frac{\rho_\infty}{\rho_2} - \bar{Q}}{\frac{\gamma + 1}{\gamma - 1}\frac{\rho_\infty}{\rho_2} - 1} \tag{13}$$

$$\frac{\rho}{\rho_\infty} = \frac{1}{\rho_\infty/\rho_2}\left[\frac{\frac{\gamma + 1}{\gamma - 1}\frac{\rho_\infty}{\rho_2} - \bar{Q}}{\frac{\gamma + 1}{\gamma - 1}\frac{\rho_\infty}{\rho_2} - \left(\frac{\rho_\infty}{\rho_2}\right)^2}\right]^{\frac{1}{\gamma-1}} \tag{14}$$

$$\frac{p}{p_\infty} = \frac{\rho}{\rho_\infty}\frac{T}{T_\infty} \tag{15}$$

where

$$\bar{Q} = \frac{1}{\tan^2 \theta_2}\left[\left(\frac{V/V_\infty}{\cos \theta_2}\right)^2 - 1\right] \tag{16}$$

To estimate $\bar{Q}$ note that $[(V/V_\infty)/\cos \theta_2]$ can be obtained directly from equation (6) or at the cone surface from equation (10). Since it can be shown that at the surface $\bar{Q}_c = (\rho_\infty/\rho_2)^2$ and 0 for wedge and swept-cylinder flows, respectively, it is evident that $0 \leq \bar{Q} < 1$ for all conical flows.

Since real-gas flows are of practical interest, the application of equations (13) to (16) to the specific case of a real gas in thermodynamic equilibrium will be considered briefly. For simplicity, it is assumed that γ is constant, since in an actual case the variation of γ along a streamline, behind the shock, is small. An effective value of γ can be estimated from known free-stream conditions and the density ratio across the shock and is given by equation (17).

$$\gamma_E = \frac{\left(2/M_{\infty n}^2\right) - \left[(\rho_\infty/\rho_2) + 1\right]}{(\rho_\infty/\rho_2) - 1} \tag{17}$$

With γ_E known, flow properties are estimated from equations (13) to (16) by replacing γ with its effective value from (17).

RESULTS AND DISCUSSION

To demonstrate accuracy of the present approximation, the predicted results will be compared with exact numerical solutions for conical flows. Surface properties will be considered first; then the predicted distributions of V and ω will be compared. Since all surface properties of the flow may be of interest, the relative errors between them for a specified error in velocity may be pertinent and will be considered briefly. Starting with the isentropic flow relation between p_c/p_2 and V_c given by equation (18)

$$\frac{p_c}{p_2} = \left(\frac{V_m^2 - V_c^2}{V_m^2 - V_2^2}\right)^{\frac{\gamma}{\gamma-1}} \tag{18}$$

it can be shown that the relative error between p_c/p_2 and V_c may be estimated by means of equation (19).

$$\frac{d(p_c/p_2)/(p_c/p_2)}{dV_c/V_c} = -\frac{(2\gamma/\gamma - 1)(V_c/V_m)^2}{1 - (V_c/V_m)^2} \tag{19}$$

For a specified error in V_c, equation (19) predicts that the error in p_c/p_2 will numerically exceed that in V_c if $V_c/V_m > \sqrt{(\gamma-1)/(3\gamma-1)}$ whereas if $V_c/V_m < \sqrt{(\gamma-1)/(3\gamma-1)}$ the converse is true. Moreover, it can be shown that errors in p_c/p_2 are greater than in ρ_c/ρ_2, T_c/T_2, and c_c/c_2 in the respective proportions $(2\gamma/\gamma - 1)$ to $(2/\gamma - 1)$, 2, and 1. Therefore, a comparison of predicted V_c and p_c with exact solutions should suffice to give an upper bound on errors in most flow properties of interest. This comparison will be made on a limited basis since only solutions for conical flows generated by right-circular cones are available in a form suitably accurate for comparison. Later other conical flows will be compared with experiment.

Comparison of Predicted Surface Properties With Inviscid Numerical Solutions

Results from the approximation will be compared initially with axisymmetric solutions and then comparisons will be made for $\alpha > 0^{\circ}$.

Comparisons with axisymmetric solutions- Surface velocity and pressure will be compared with results from solutions given by references 1, 2, and 9. References 1 and 2 give tabulated results from numerical solutions of the Taylor-Maccoll equation for conical flow, while reference 9 provides solutions by the method of characteristics. The present approximation is compared with solutions by Sims (ref. 1) for $\gamma = 1.4$ in figure 5. Here the approximations for V_c and p_c are ratioed to exact values, and constant values of these ratios are shown as contours of accuracy for $0 \leq \delta_c \leq 30^{\circ}$ and $1.5 \leq M_{\infty} \leq 20$. In like manner comparisons are shown in figure 6 with solutions by Kopal (ref. 2) for $\gamma = 1.405$ and 1.333. These comparisons are made for $5^{\circ} \leq \delta_c \leq 50^{\circ}$ but are limited to $1 \leq M_{\infty} \leq 12$ because the number of solutions given was insufficient to define accuracy contours at greater M_{∞}.

Figures 5 and 6 demonstrate that accuracy of the approximation improves significantly with increasing M_{∞}. In general for $M_{\infty} \geq 5$ and $\delta_c \leq 50^{\circ}$ velocity is predicted within 0.1 percent and, except for $\delta_c \leq 5^{\circ}$, pressure is predicted within 1 percent. While accuracy is minimum for small cone angles ($\delta_c < 5^{\circ}$) inaccuracies accrue also as δ_c approaches shock wave detachment. Rigorous comparisons at detachment could not be made since available numerical solutions are given graphically; however, comparison with the method of reference 10 for $M_{\infty} = \infty$ and $1.67 \leq \gamma \leq 1.2$ indicate agreement with present predictions of velocity and pressure to about four significant figures. The present approximation appears least accurate as $M_{\infty} \rightarrow 1$. From a comparison with results from reference 1 for $M_c = 1$ figure 7 shows that predicted velocity and pressure have minimum accuracy at $M_{\infty} = 1.06$ where both are in error about 5 percent.

Figure 6 shows that decreasing the specific-heat ratio improves accuracy significantly except when M_{∞} is small. The effects of specific-heat ratio were investigated in more detail and are shown in figure 8 where comparisons are made with solutions by the method of characteristics (ref. 9). Figure 8 shows that accuracy of the approximation improves as $\gamma \rightarrow 1$ for a wide range of cone angles. The applicability of the approximation to flows of a real gas in equilibrium for a range of γ_E is demonstrated in figure 9. Here the pressure ratio p_c/p_2 is compared with exact solutions by the method of reference 9. For the specified free-stream conditions, figure 9 indicates that predicted values of p_c/p_2 agree with exact solutions to within 0.5 percent.

Comparisons with solutions for $\alpha > 0^{\circ}$- A critical assessment of how well the approximation applies to the more general case $\alpha > 0^{\circ}$ can be made by a comparison of predicted distributions of the velocity component ϵ_c with exact numerical solutions of conical flow from reference 4. As shown in

figure 4 ϵ_c is the incremental value that V_c exceeds the local velocity for swept-cylinder flow having the same θ_2 and local $\omega = \omega_c$ and is given by equation (20).

$$\epsilon_c = V_c - V_\infty \left[\frac{\cos \theta_2}{\cos(\theta_2 - \omega_c)}\right] \tag{20}$$

Results from cross plotting numerical solutions with θ_2 constant but varying δ_c and α are compared with the approximation in figure 10. Here ϵ_c/V_∞ is presented as a function of $\tan(\theta_2 - \omega_c)/\tan(\theta_2 - \omega_2)$ as an abscissa. From figure 4 it can be seen that this abscissa is the fraction of the velocity component from point s to 2 to where V_c crosses this component.

Figure 10 shows that exact distributions of ϵ_c/V_∞ agree well with predicted distributions and moreover for specified M_∞ tend to give a single distribution as predicted by the approximation. The condition for ϵ_c/V_∞ to be maximum is predictable from the present approximation by equating $d\epsilon_c/d[\tan(\theta_2 - \omega_c)/\tan(\theta_2 - \omega_2)]$ to zero and is given by equation (21).

$$\tan^2(\theta_2 - \omega_2)\left[\frac{\tan(\theta_2 - \omega_c)}{\tan(\theta_2 - \omega_2)}\right]^4 + 2\left[\frac{\tan(\theta_2 - \omega_c)}{\tan(\theta_2 - \omega_2)}\right] - 1 = 0 \tag{21}$$

Figure 10 shows good agreement between the predicted maximum and exact solutions.

The approximations for V_c and p_c are compared with conical-flow solutions for $\alpha \geq 0^\circ$ from reference 4 in figure 11. Velocity and pressure are normalized by exact values and are shown as functions of the inclination of the stagnation line ω_c. Comparisons are made for both windward and leeward stagnation lines, and since for the windward side $\omega_c = \delta_c + \alpha$ while for the leeward side $\omega_c = \delta_c - \alpha$, the demarcation between these two cases is apparent in figure 11 when $\omega_c = \delta_c$. Trends of accuracy indicated in figure 11 appear consistent with those previously demonstrated for axisymmetric flow, and generally good agreement of predicted and exact results is demonstrated.

A more practical demonstration of the usefulness of the approximation is afforded by the direct comparison of predicted pressure ratio p_c/p_2 with exact values shown in figure 12. Also shown are pressure ratios for wedge and swept-cylinder flows which are obtained from the approximation as special limiting cases. It is evident from figure 12 that for $\alpha > 0^\circ$ the approximation provides good accuracy for a wide range of conical flows.

Comparisons of Predicted Distributions of Velocity and Flow Angle With Inviscid Solutions

Axisymmetric distributions of velocity and flow angle given by equations (7) and (11), respectively, are compared with exact solutions in figure 13. Likewise for $\alpha > 0^\circ$, distributions in the angle-of-attack plane are compared in figure 14. From figure 13 it can be seen that, in accordance with the predictions of surface properties, the predicted distributions of velocity and flow angle are least accurate at small δ_c. In general, if surface properties are predicted accurately then distributions will also be accurate. It should be noted that while figure 13 shows significant differences between predicted and exact distributions for small δ_c the actual differences in flow properties are not large. For example, the greatest difference in flow angle between predicted and exact values shown by the distributions of figure 13 is only about 1° for $\delta_c = 2.5^\circ$.

Comparisons of the Approximation With Experiment

Comparisons with experiment are, of necessity, limited to investigations from which both θ_2 and p_c (or some other flow property) can be evaluated. Accordingly, results from references 11 to 14 have been selected for comparisons with the approximation. These investigations encompass a range of Mach numbers from about 5 to 15. It is clear from previous inviscid comparisons that for circular cones at small α at least, any significant differences between the approximation and experiment for this range of M_∞ must be attributed mainly to viscous effects and inaccuracies in the evaluation of θ_2 and p_c rather than to the small errors inherent in the approximation. Except for results from reference 11, shock angles were measured from shadowgraphs of the flow; shock angles from reference 11 were estimated from pitot traverses of shock layers. These traverses also afford an estimate of boundary-layer thickness; therefore, the effects of boundary-layer displacement were accounted for approximately by measuring surface inclination ω_c to the boundary-layer edge, and to the shear line of the lee separated flow. On the other hand, results from references 12 to 14 are compared on the basis of ω_c measured from the cone surface and are denoted inviscid. In addition, for these cases ω_c was arbitrarily increased 1° to show the effect of boundary layer displacement. For all cases, pressure was measured at the cone surface and the pressure ratio p_c/p_2 has, therefore, been selected as a basis for comparison.

In figure 15 p_c/p_2 predicted by the approximation is compared with results from references 11 and 12 for a 15° semiapex cone. The agreement between experiment and the approximation is reasonable for both air and helium on the windward surface; but on the leeward side, greater differences are indicated for air (fig. 15(a)), probably because of difficulty in accurately measuring p_c. A similar comparison is shown in figure 16 with experimental results from reference 13 for $\delta_c = 5^\circ$. While the approximation appears to generally underestimate p_c/p_2, reasonably good agreement is indicated for $5^\circ \leq \omega_c \leq 45^\circ$.

Comparisons for an elliptic cone for two different ratios of major-to-minor axes are shown in figure 17 from results given in reference 14. Although the approximation underestimates experimental values slightly, good agreement is indicated for a wide range of ω_c. The approximation appears reasonably valid even at large ω_c where θ_2 has the strong shock solution and the flow in the shock layer is subsonic and therefore affected by the model base. Since the shock waves appear straight in the shadowgraphs of reference 14, even when $M_c < 1$, it is apparent that the flow continues to be nearly conical even though model length is finite. Moreover, shadowgraphs of a 15° semiapex cone in helium at $M_\infty \simeq 15$ shown in figure 18 demonstrate that the shocks tend to remain essentially straight even though $\theta_2 \to 90°$. It appears from these results that if the body is sufficiently slender the flow remains nearly conical near the apex even at large α and the approximation can be applied.

CONCLUDING REMARKS

An approximation is developed for the distribution of flow properties in the angle-of-attack plane of conical flows. It is assumed that shock angle and surface inclination are known and the flow is inviscid and isentropic. Comparisons of the approximation with exact solutions and experiment demonstrate applicability for a wide range of conical flows. Equations are presented from which estimates of flow properties can be made.

Ames Research Center
National Aeronautics and Space Administration
Moffett Field, Calif., 94035, April 23, 1970

APPENDIX A

DERIVATION OF EQUATIONS FOR DISTRIBUTIONS OF VELOCITY AND FLOW ANGLE

PROPERTIES OF THE CIRCULAR ARC APPROXIMATION

The purpose of this appendix is to derive explicit equations for distributions of velocity and flow angle by approximating the streamline hodographs of axisymmetric conical flows by circular arcs. Pertinent velocity vectors and angles are shown in sketch (a). The center of the circular arc with radius $\bar{R}$ is at the point $(\bar{H}, \bar{K})$ which is the intersection of an extension of V_c and a normal to the component 2-s at point 2. By constructing a normal to V_c that passes through point 2 and by resolving components it is evident that

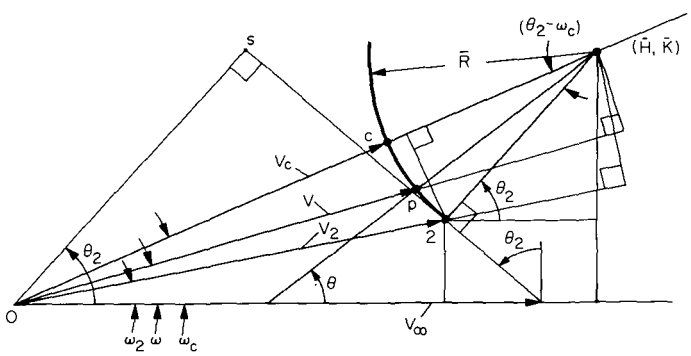

Sketch (a)

$$\bar{R} \sin(\theta_2 - \omega_c) = V_2 \sin(\omega_c - \omega_2) \tag{A1}$$

and since

$$V_2 = V_\infty \frac{\cos \theta_2}{\cos(\theta_2 - \omega_2)} \tag{A2}$$

it follows that

$$\bar{R} = V_\infty \frac{\cos \theta_2 \sin(\omega_c - \omega_2)}{\cos(\theta_2 - \omega_2)\sin(\theta_2 - \omega_c)} \tag{A3}$$

In addition

$$\bar{H} = V_2 \cos \omega_2 + \bar{R} \cos \theta_2 \tag{A4}$$

$$\bar{K} = V_2 \sin \omega_2 + \bar{R} \sin \theta_2 \tag{A5}$$

Substituting (A2) and (A3) in both (A4) and (A5) and employing known trigonometric identities yields (A6) and (A7), respectively.

$$\bar{H} = V_\infty \frac{\tan(\theta_2 - \omega_2)}{\sin(\theta_2 - \omega_c)} \cos \theta_2 \cos \omega_c \tag{A6}$$

$$\bar{K} = V_\infty \frac{\tan(\theta_2 - \omega_2)}{\sin(\theta_2 - \omega_c)} \cos\theta_2 \sin\omega_c \tag{A7}$$

Velocity as a Function of $(\omega_c - \omega)$

The equation of the circular arc is given by (A8).

$$(u - \bar{H})^2 + (v - \bar{K})^2 = \bar{R}^2 \tag{A8}$$

Substitution of $u = V\cos\omega$ and $v = V\sin\omega$ in equation (A8) yields the quadratic equation in V given by (A9)

$$V^2 - 2(\bar{H}\cos\omega + \bar{K}\sin\omega)V + \bar{H}^2 + \bar{K}^2 - \bar{R}^2 = 0 \tag{A9}$$

Substituting equations (A3), (A6), and (A7) for $\bar{R}$, $\bar{H}$, and $\bar{K}$, respectively, in equation (A9), solving the quadratic, and employing trigonometric identities yields V/V_∞ as a function of $(\omega_c - \omega)$ and this is given by equation (A10).

$$\frac{V}{V_\infty} = \frac{\cos\theta_2 \tan(\theta_2 - \omega_2)}{\sin(\theta_2 - \omega_c)} \left\{ \cos(\omega_c - \omega) - \left[\cos^2(\omega_c - \omega) - 1 + \frac{\sin^2(\omega_c - \omega_2)}{\sin^2(\theta_2 - \omega_2)} \right]^{1/2} \right\} \tag{A10}$$

It is apparent that the minus sign before the radical is the appropriate choice here since the plus sign yields velocity to the opposite side of the circle.

Flow Angle as a Function of $(\theta - \omega_c)$

By erecting normals through the point $\bar{H}$ and $\bar{K}$ to extensions of V and V_2, and resolving components it can be shown that equation (A11) applies

$$\sin(\theta_2 - \omega_2)\sin(\omega_c - \omega) = \sin(\omega_c - \omega_2)\sin(\theta - \omega) \tag{A11}$$

Equation (A11) can be recast[1] as (A12) where $(\omega_c - \omega)$ is an explicit function of the conical coordinate $(\theta - \omega_c)$

$$\cos(\omega_c - \omega) = \frac{1 - B\cos(\theta - \omega_c)}{[B^2 + 1 - 2B\cos(\theta - \omega_c)]^{1/2}} \tag{A12}$$

---

[1]Note that $\sin(\theta - \omega) = \sin[(\theta - \omega_c) + (\omega_c - \omega)]$.

and where

$$B = \frac{\sin(\omega_c - \omega_2)}{\sin(\theta_2 - \omega_2)} \tag{A13}$$

A simpler alternate for (A12) is given by (A14)

$$\omega_c - \omega = \tan^{-1}\left[\frac{B \sin(\theta - \omega_c)}{1 - B \cos(\theta - \omega_c)}\right] \tag{A14}$$

Velocity as a Function of $(\theta - \omega_c)$

Substitution of (A12) in (A10) yields V/V_∞ as a function of the conical coordinate $(\theta - \omega_c)$ and this is given by equation (A15)

$$\frac{V}{V_\infty} = \cos\theta_2\left[\tan(\theta_2 - \omega_2)\tan\frac{1}{2}(\theta_2 - \omega_c) + 1\right]\left\{1 + \frac{2B}{(1 - B)^2}[1 - \cos(\theta - \omega_c)]\right\}^{1/2} \tag{A15}$$

Using oblique-shock theory in conjunction with an alternate equation for B, equation (A15) can be recast independent of ω_2. From oblique-shock equations given in reference 8 it can be shown that equation (A16) applies[2]

$$\tan(\theta_2 - \omega_2) = \frac{\rho_\infty}{\rho_2}\tan\theta_2 \tag{A16}$$

where

$$\frac{\rho_\infty}{\rho_2} = \frac{2}{\gamma + 1}\left(\frac{1}{M_{\infty_n}^2} + \frac{\gamma - 1}{2}\right) \tag{A17}$$

A combination of equation (A16) with an expansion of (A13) yields equation (A18) which is independent of ω_2.

$$B = \cos(\theta_2 - \omega_c) - \frac{\sin(\theta_2 - \omega_c)}{(\rho_\infty/\rho_2)\tan\theta_2} \tag{A18}$$

Substitution of (A16) in (A15) with B given by equation (A18) yields equation (A19) which is independent of ω_2.[3]

---

[2]From equation (A16) and figure 4 it is evident that ρ_∞/ρ_2 equals the ratio of the velocity component s - 2 to the free-stream component normal to the shock wave.

[3]Equation (A14) is made independent of ω_2 by using (A18) for B.

$$\frac{V}{V_\infty} = \cos\theta_2 \left[\frac{\rho_\infty}{\rho_2} \tan\theta_2 \tan\frac{1}{2}(\theta_2 - \omega_c) + 1\right]\left\{1 + \frac{2B}{(1-B)^2}[1 - \cos(\theta - \omega_c)]\right\}^{1/2} \tag{A19}$$

At the cone surface $\theta = \omega_c$ and equation (A19) reduces to (A20).

$$\frac{V_c}{V_\infty} = \cos\theta_2 \left[\frac{\rho_\infty}{\rho_2} \tan\theta_2 \tan\frac{1}{2}(\theta_2 - \omega_c) + 1\right] \tag{A20}$$

Equation (A19) when divided by equation (A20) yields velocity distribution normalized by V_c and this is given by equation (A21)

$$\frac{V}{V_c} = \left\{1 + \frac{2B}{(1-B)^2}[1 - \cos(\theta - \omega_c)]\right\}^{1/2} \tag{A21}$$

APPENDIX B

COMPATIBILITY OF THE APPROXIMATION WITH WEDGE AND SWEPT-CYLINDER FLOWS

Equation (B1) (identically eq. (5)) will be examined to verify that distributions of V/V_∞ for wedge and swept-cylinder flows are contained as special cases.

$$\frac{V}{V_\infty} = \frac{\cos\theta_2 \tan(\theta_2 - \omega_2)}{\sin(\theta_2 - \omega_c)} \left\{ \cos(\omega_c - \omega) - \left[\cos^2(\omega_c - \omega) - 1 + \frac{\sin^2(\omega_c - \omega_2)}{\sin^2(\theta_2 - \omega_2)} \right]^{1/2} \right\} \tag{B1}$$

For wedge flow $\omega_c = \omega_2 = \omega$ and substitution in equation (B1) gives $V/V_\infty = \cos\theta_2/\cos(\theta_2 - \omega_2) = V_2/V_\infty$ which is the exact result (see fig. 4).

For swept cylinders $\omega_c = \theta_2$ and substitution in equation (B1) gives an indeterminate form since the outer bracketed quantity and the denominator are both zero. An evaluation can be made by allowing

$$F = \sin(\theta_2 - \omega_c) \tag{B2}$$

and

$$f = \left\{ \cos(\omega_c - \omega) - \left[\cos^2(\omega_c - \omega) - 1 + \frac{\sin^2(\omega_c - \omega_2)}{\sin^2(\theta_2 - \omega_2)} \right]^{1/2} \right\} \tag{B3}$$

and evaluating

$$\lim_{\omega_c \to \theta_2} \frac{df/d\omega_c}{dF/d\omega_c} \tag{B4}$$

Performing the indicated operation gives

$$\lim_{\omega_c \to \theta_2} \frac{-1}{\cos(\theta_2 - \omega_c)} \left[\frac{-\cos(\theta_2 - \omega_2)}{\cos(\theta_2 - \omega)\sin(\theta_2 - \omega_2)} \right] = \left[\frac{\cos(\theta_2 - \omega_2)}{\cos(\theta_2 - \omega)\sin(\theta_2 - \omega_2)} \right] \tag{B5}$$

and

$$\frac{V}{V_\infty} = \cos\theta_2 \tan(\theta_2 - \omega_2) \left[\frac{\cos(\theta_2 - \omega_2)}{\cos(\theta_2 - \omega)\sin(\theta_2 - \omega_2)} \right] \tag{B6}$$

Equation (B6) can be reduced to

$$\frac{V}{V_\infty} = \frac{\cos \theta_2}{\cos(\theta_2 - \omega)}$$

which can be recognized as the exact expression for swept-cylinder flow from figure 4.

REFERENCES

1. Sims, Joseph L.: Tables for Supersonic Flow Around Right-Circular Cones at Zero Angle of Attack. NASA SP-3004, 1964.

2. Staff of the Computing Section (under the direction of Zdeněk Kopal): Tables of Supersonic Flow Around Cones. Tech. Rep. 1, Mass. Inst. Tech., Dept. Electrical Engr., Center of Analysis, 1947.

3. Henderson, Arthur, Jr.; and Braswell, Dorothy O.: Charts for Conical and Two-Dimensional Oblique-Shock Flow Parameters In Helium at Mach Numbers From About 1 to 100. NASA TN D-819, 1961.

4. Babenko, K. I.; Voskresenskiy, G. P.; Lyubimov, A. N.; and Rusanov, V. V.: Three-Dimensional Flow of Ideal Gas Past Smooth Bodies. NASA TT-F-380, 1966.

5. Jones, D. J.: Tables of Inviscid Supersonic Flow About Circular Cones at Incidence $\gamma = 1.4$. Parts I and II. Agardograph 137, Nov. 1969.

6. Shapiro, Ascher H.: The Dynamics and Thermodynamics of Compressible Fluid Flow. Vol. 2, The Ronald Press, N. Y., 1954.

7. Hantzsche, W.; and Wendt, H.: Cones in Supersonic Flow. NACA TM 1157, 1947.

8. Ames Research Staff: Equations, Tables, and Charts for Compressible Flow. NACA Rep. 1135, 1953.

9. Rakich, John V.: Numerical Calculation of Supersonic Flows of a Perfect Gas Over Bodies of Revolution at Small Angles of Yaw. NASA TN D-2390, 1964.

10. Cleary, Joseph W.: Wedge and Cone Theory for $M_\infty = \infty$. Technical Comment. AIAA J., vol. 3, Oct. 1965, pp. 1983-84.

11. Cleary, Joseph W.: Effects of Angle of Attack and Bluntness on the Shock-Layer Properties of a 15° Cone at a Mach Number of 10.6. NASA TN D-4909, 1968.

12. Cleary, Joseph W.; and Duller Charles E.: Effects of Angle of Attack and Bluntness on the Hypersonic Flow Over a 15° Semiapex Cone in Helium. NASA TN D-5903, 1970.

13. Feldhuhn, Robert H.; and Winkelmann, Allen E.: Separated Flow Phenomena on a Slender Cone at Mach 5. Final Report ARPA Order-905, NOLTR-69-36, March 1969.

14. Palko, R. L.; and Ray, A. D.: Pressure Distribution and Flow Visualization Tests of a 1.5 Elliptic Cone at Mach 10. AEDC-TDR-63-163, August 1963.

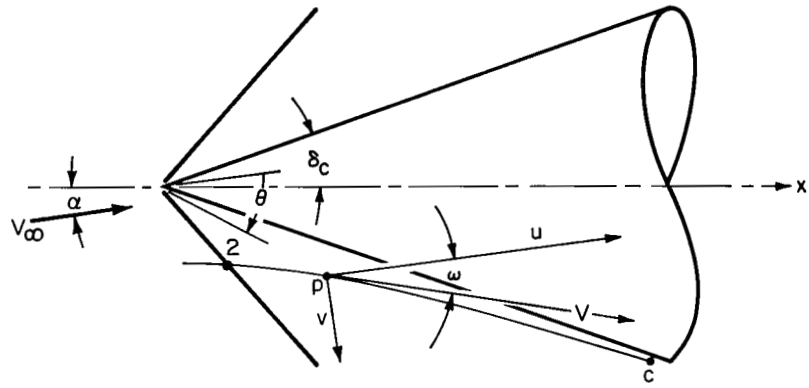

Figure 1.- Example of inviscid conical flow.

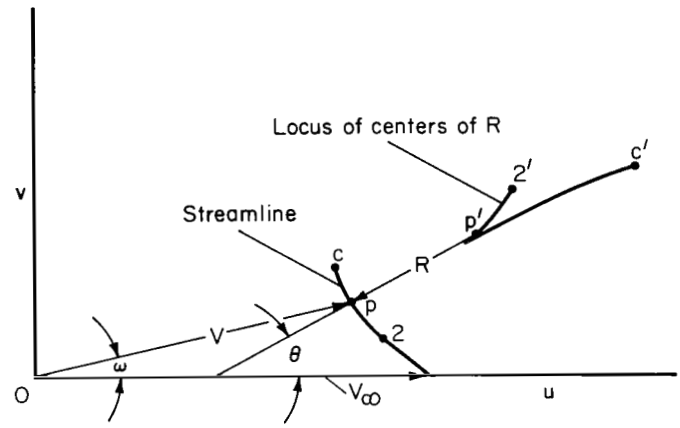

Figure 2.- Streamline hodograph of a typical axisymmetric conical flow.

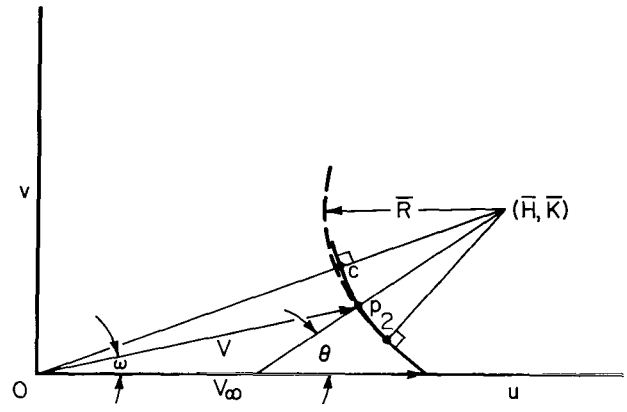

Figure 3.- Approximation for the streamline hodograph.

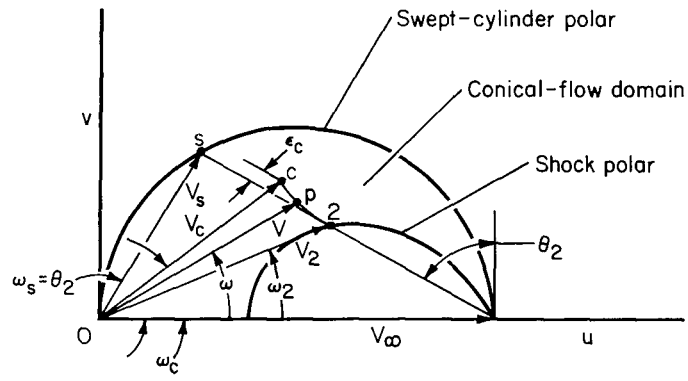

Figure 4.- Hodographs of typical conical flows.

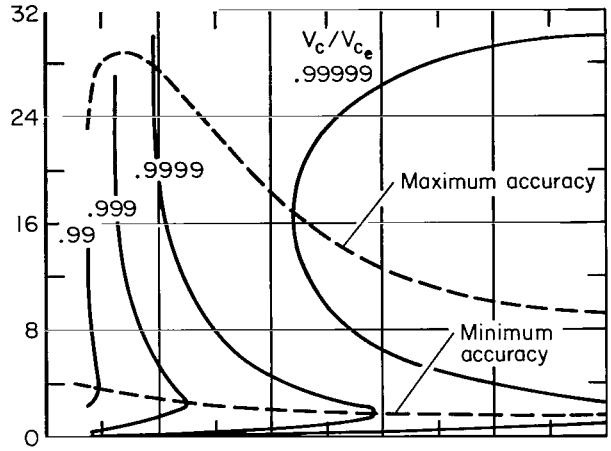

(a) Velocity ratio.

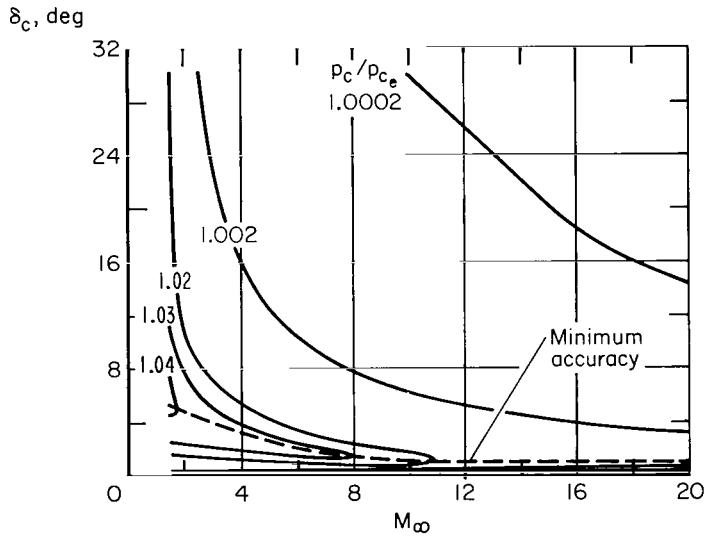

(b) Pressure ratio.

Figure 5.- Accuracy contours of the approximation from comparisons with exact solutions of reference 1; $\alpha = 0^o$.

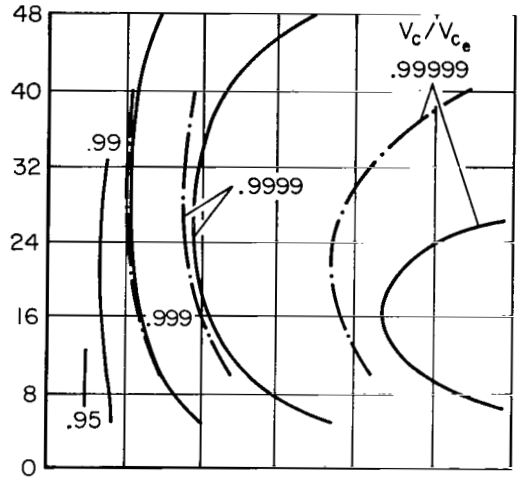

(a) Velocity ratio.

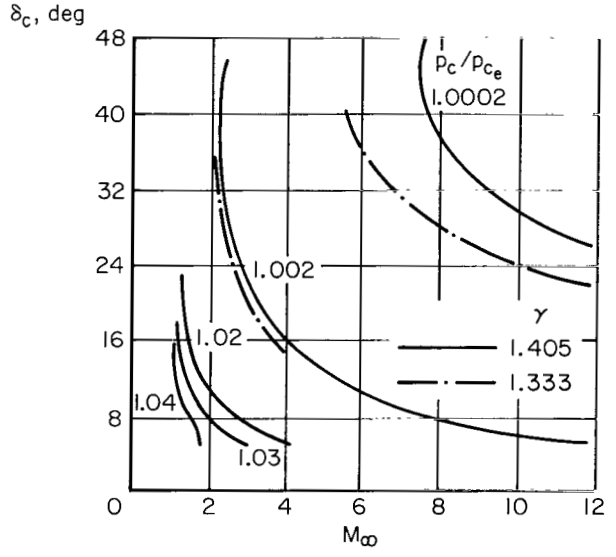

(b) Pressure ratio.

Figure 6.- Accuracy contours of the approximation from comparisons with exact solutions of reference 2; $\alpha = 0^o$.

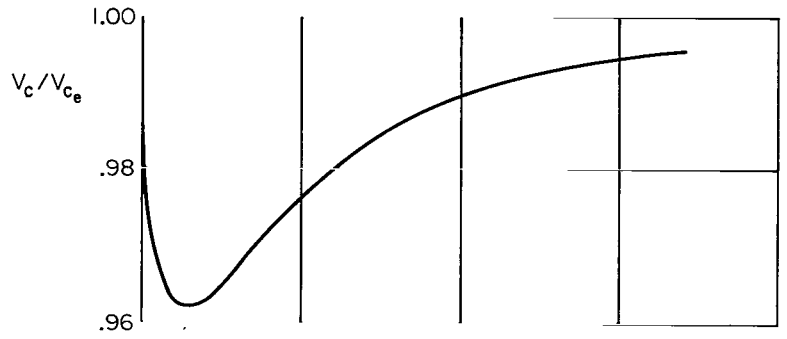

(a) Velocity ratio.

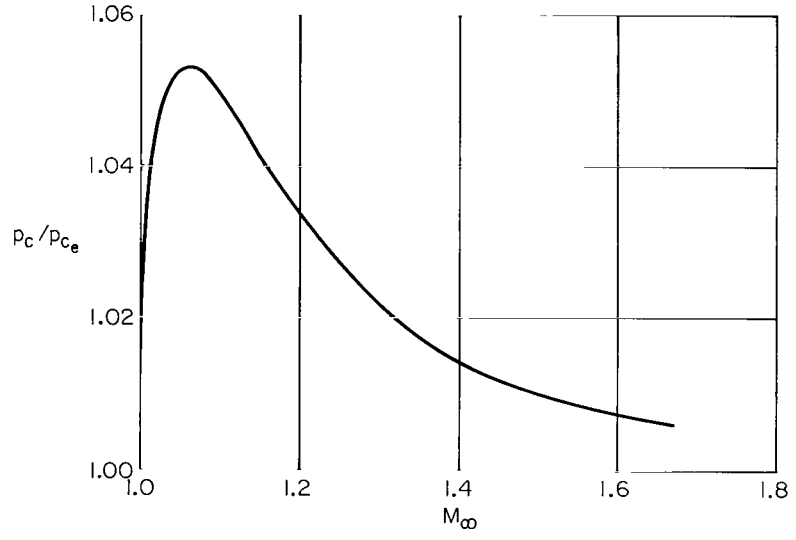

(b) Pressure ratio.

Figure 7.- Comparison of the approximation with exact solutions from reference 1 with $M_c = 1$; $\alpha = 0^o$.

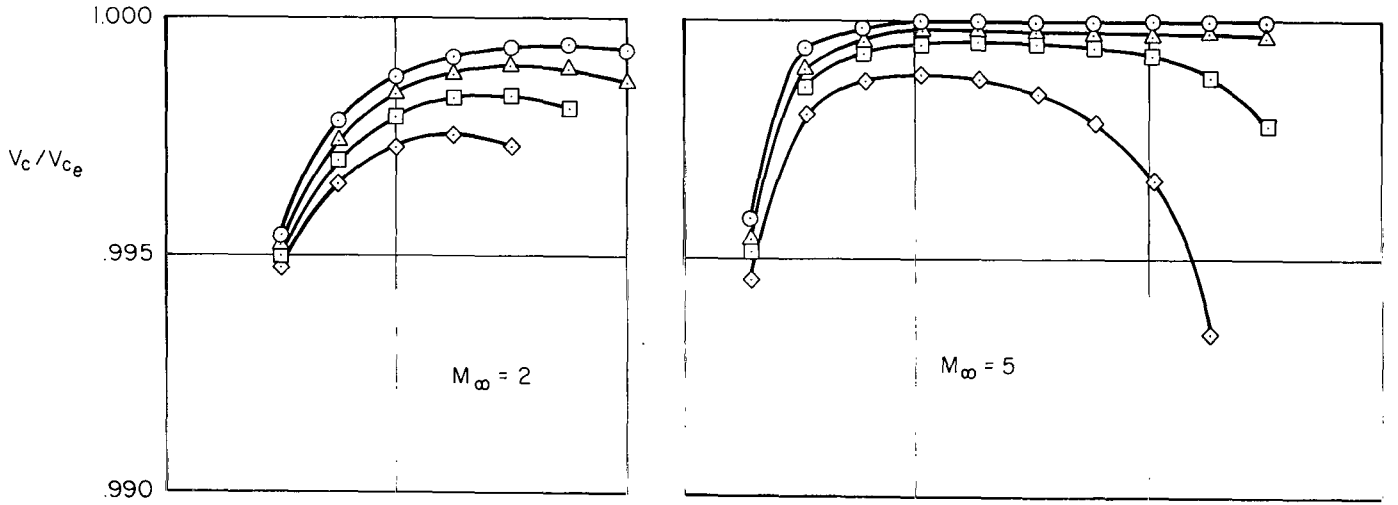

(a) Velocity ratio.

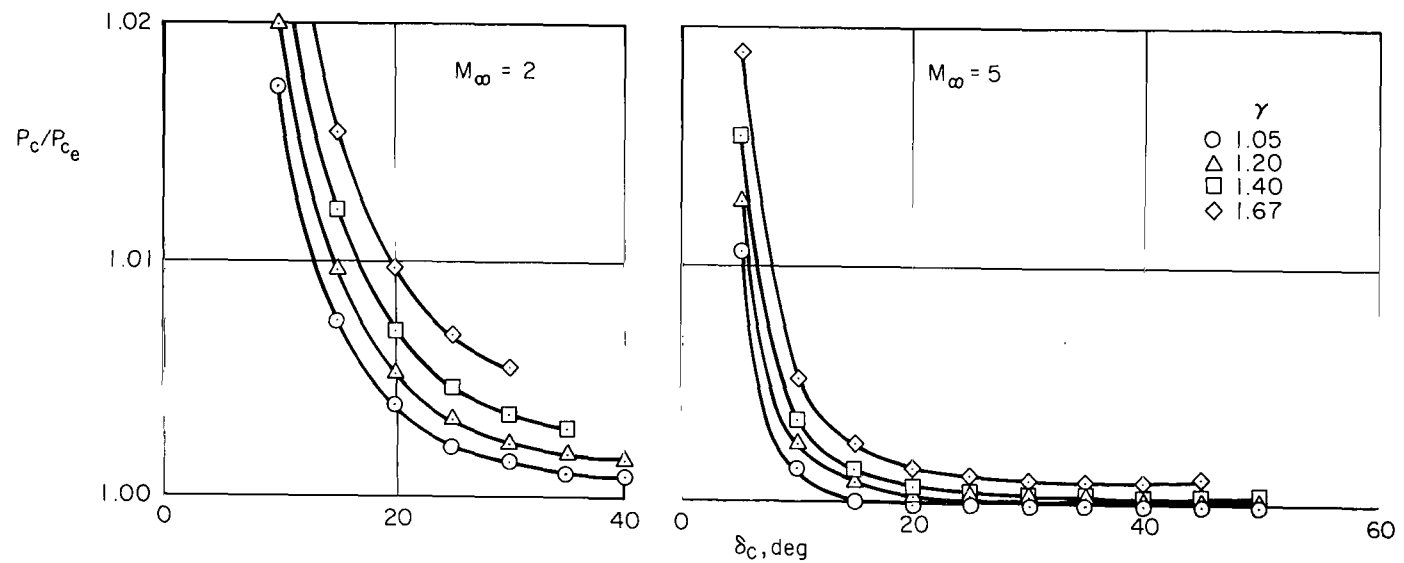

(b) Pressure ratio.

Figure 8.- Comparison of the approximation with exact solutions from reference 9; $\alpha = 0^o$.

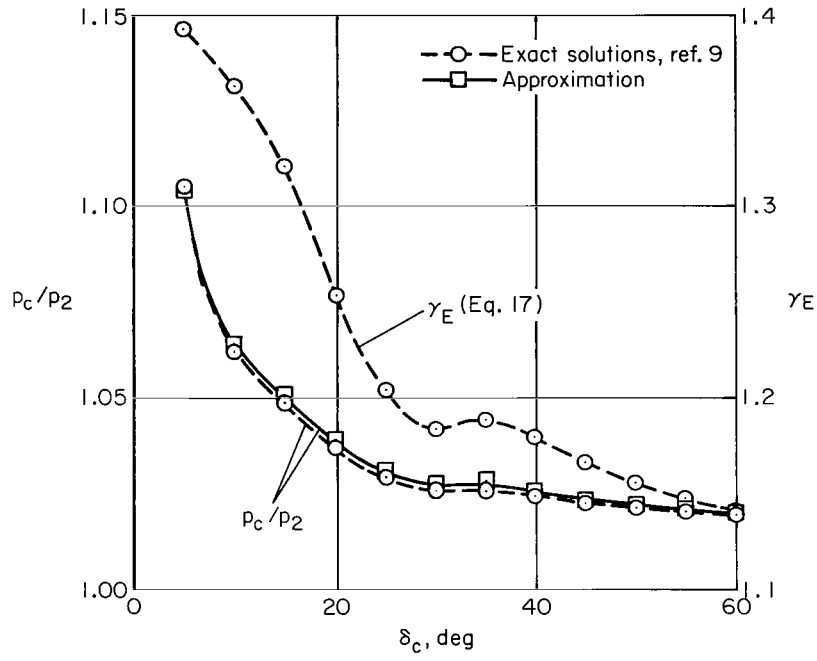

Figure 9.- Comparison of the approximation with real gas solutions for air in thermodynamic equilibrium; $M_\infty = 20$, $V_\infty = 23{,}414$ ft/sec, $P_\infty = 1$ lb/sq ft, $\alpha = 0^\circ$.

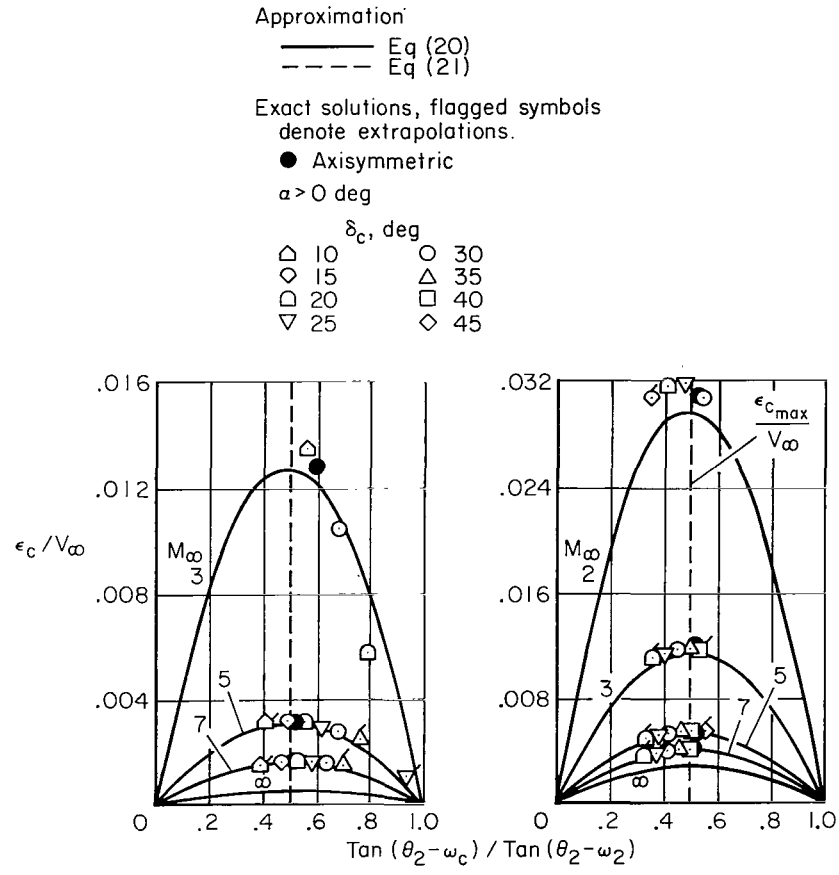

(a) $\theta_2 = 22.5^\circ$ (b) $\theta_2 = 48^\circ$

Figure 10.- Comparison of approximate incremental velocity with exact solutions from reference 4.

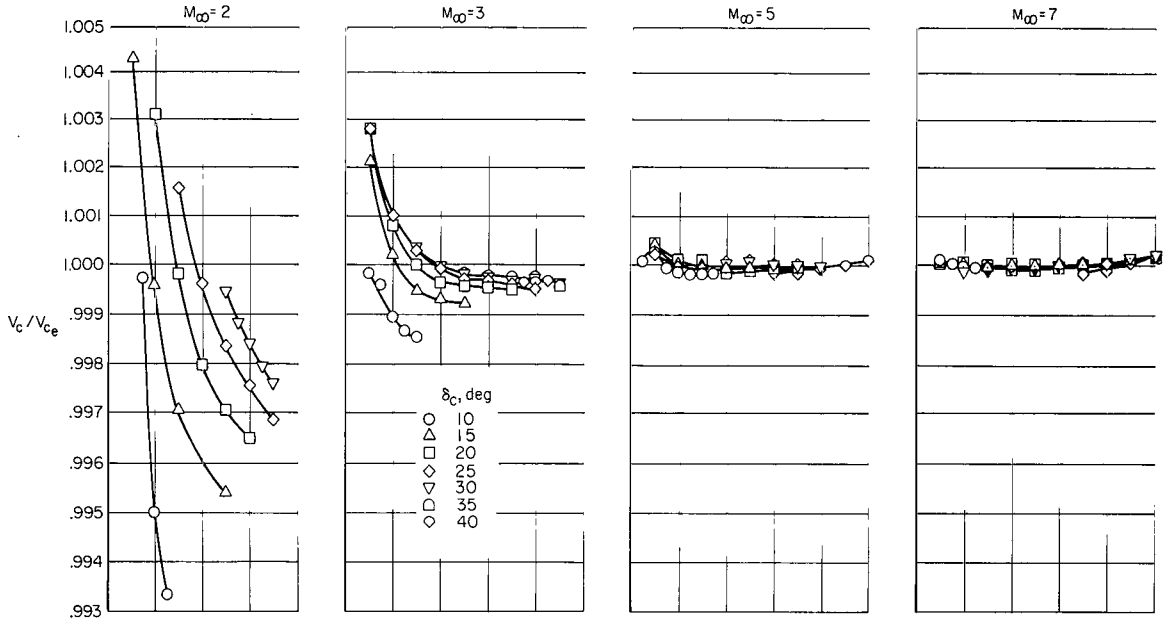

(a) Velocity ratio.

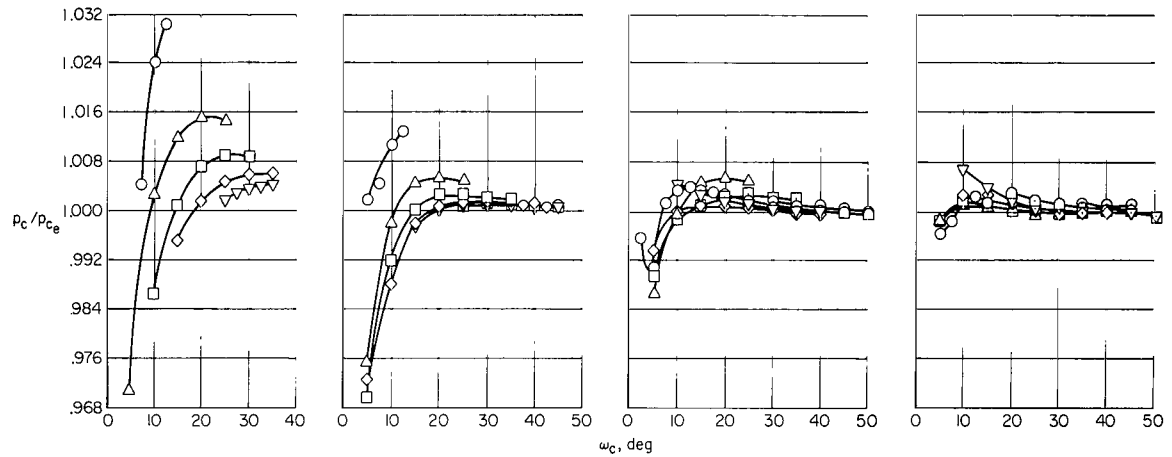

(b) Pressure ratio.

Figure 11.- Comparison of the approximation with exact solutions from reference 4; $\alpha \geq 0^\circ$.

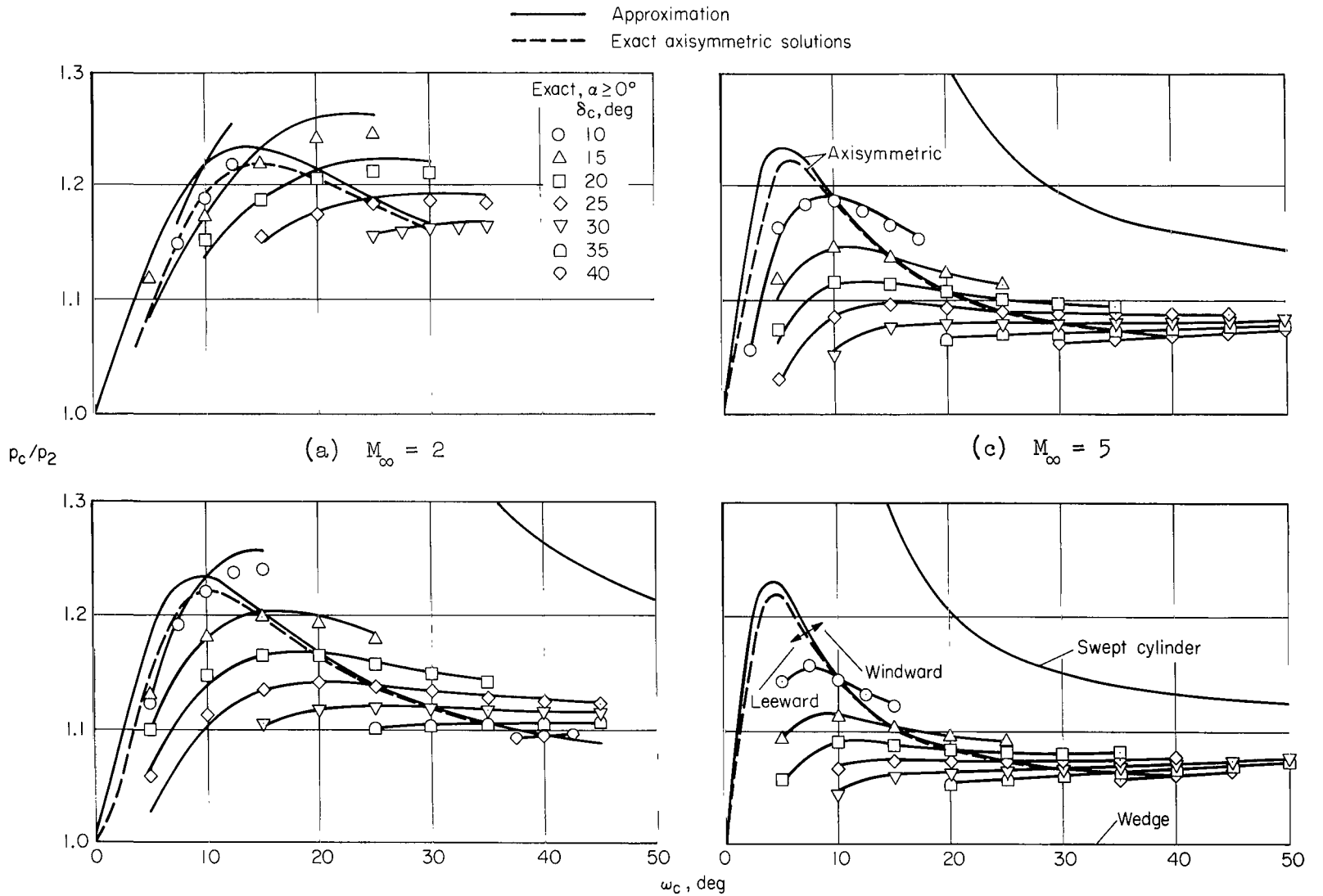

(a) $M_\infty = 2$

(b) $M_\infty = 3$

(c) $M_\infty = 5$

(d) $M_\infty = 7$

Figure 12.- Comparison of the approximate pressure ratio with exact solutions from reference 4 for right circular cones; $\alpha \geq 0^\circ$.

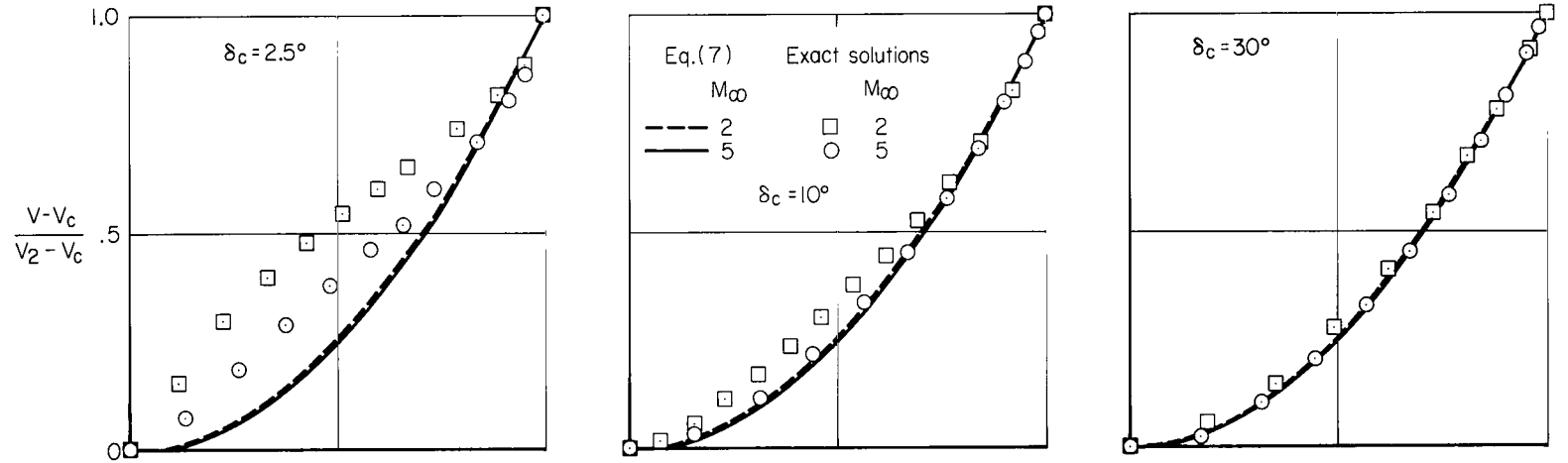

(a) Velocity.

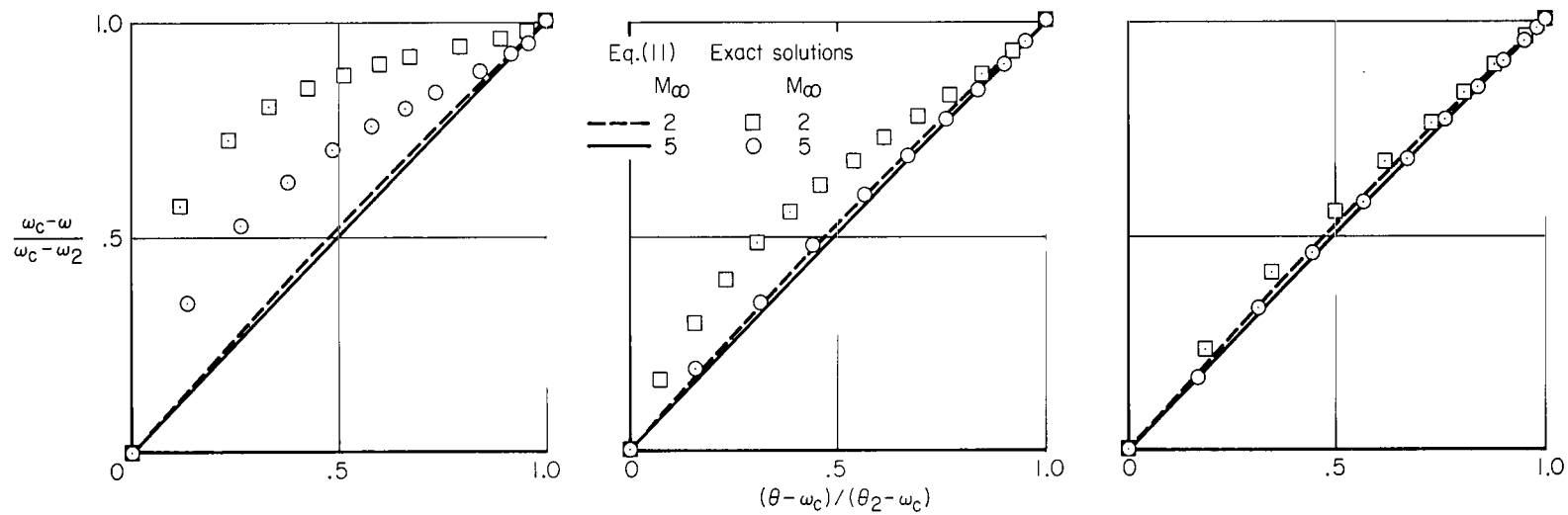

(b) Flow angle.

Figure 13.- Comparison of distributions with exact solutions from reference 1; $\gamma = 1.4$, $\alpha = 0°$.

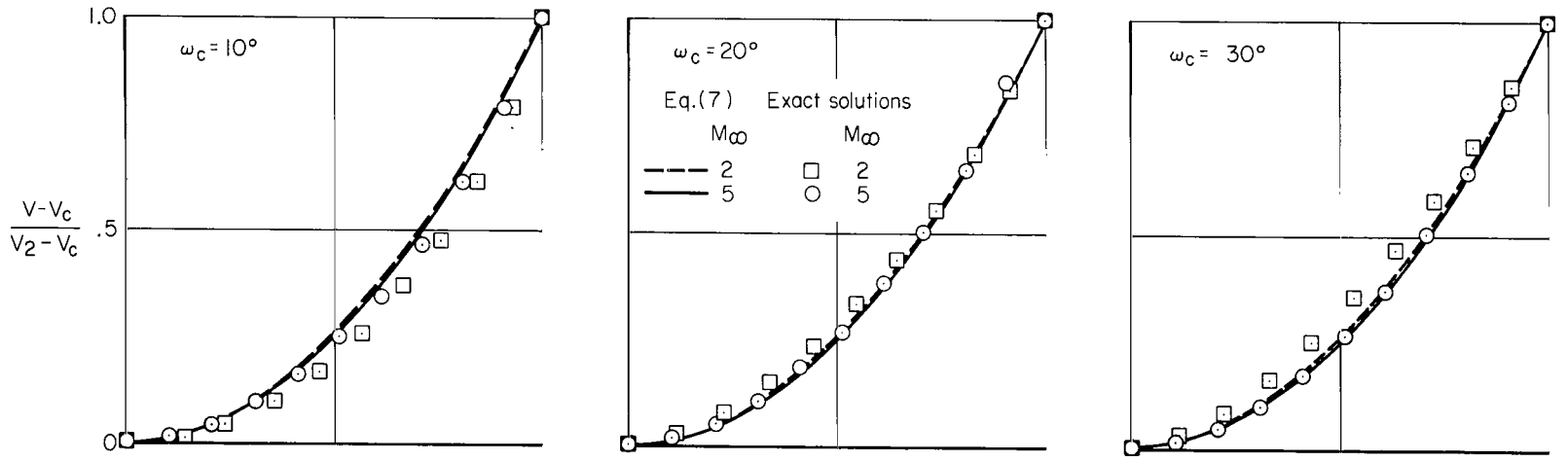

(a) Velocity.

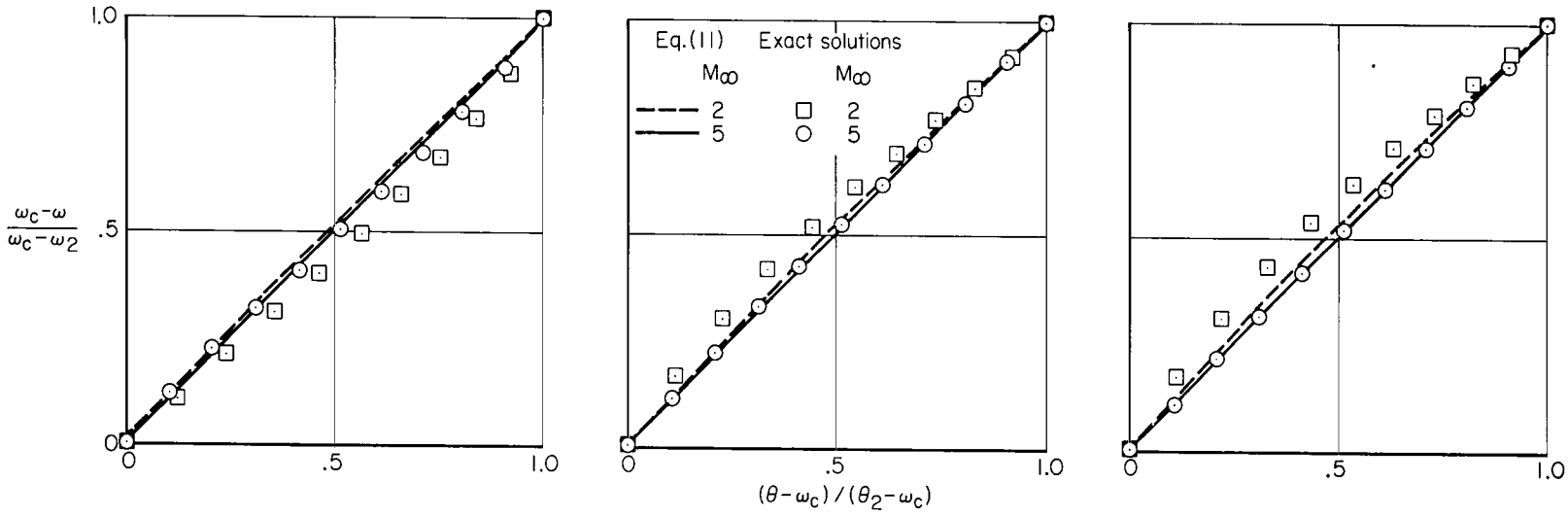

(b) Flow angle.

Figure 14.- Comparison of distributions with exact solutions from reference 4; $\gamma = 1.4$, $\alpha \geq 0°$, $\delta_c = 20°$.

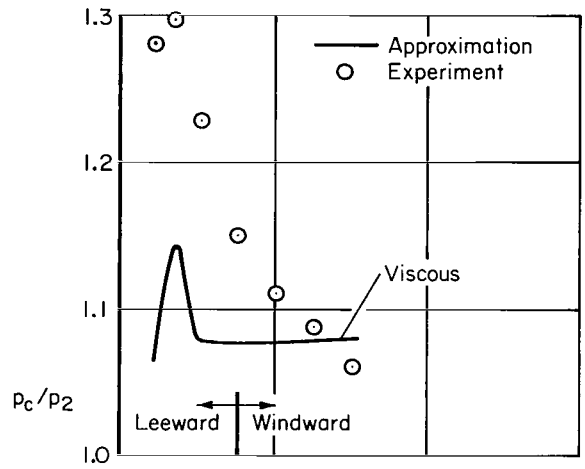

(a) $M_\infty = 10.6$; $\gamma = 1.4$, reference 11.

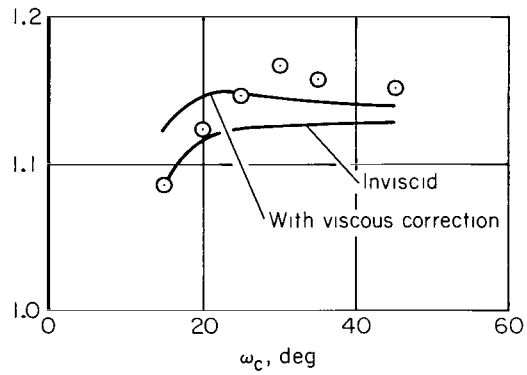

(b) $M_\infty = 14.9$; $\gamma = 1.67$, reference 12.

Figure 15.- Comparison of approximate pressure ratio with experimental values for a 15° semiapex cone.

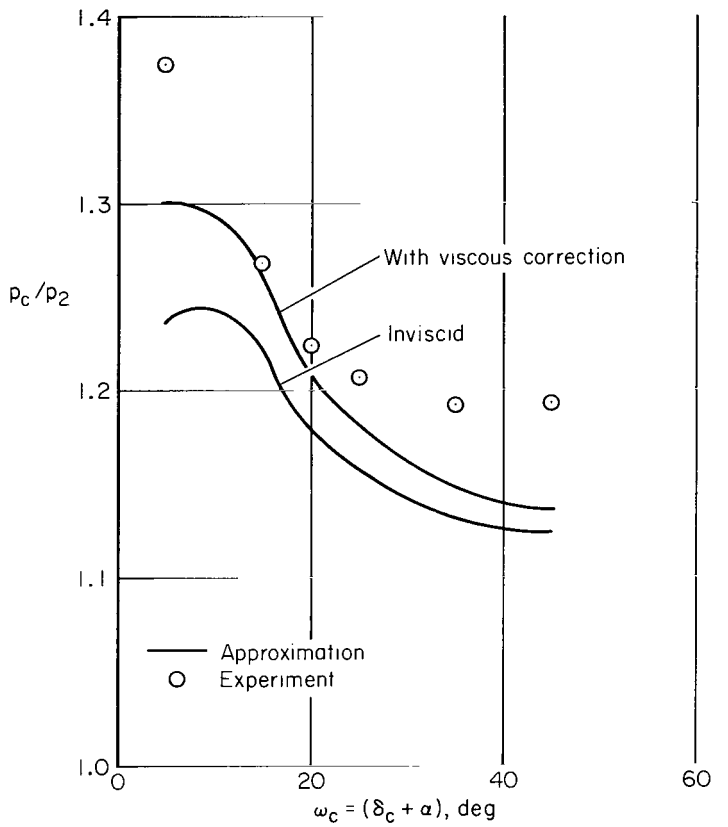

Figure 16.- Comparison of approximate pressure ratio with experimental values for a 5° semiapex cone; $M_\infty = 5.03$, $\gamma = 1.4$, reference 13.

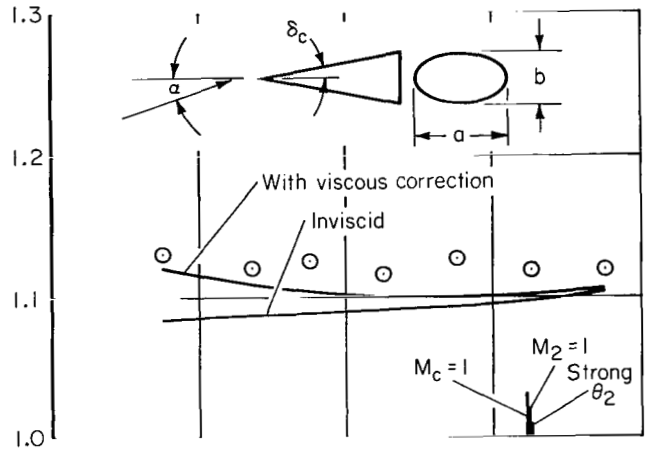

(a) $a/b = 0.667$; $\delta_c = 15.2^o$

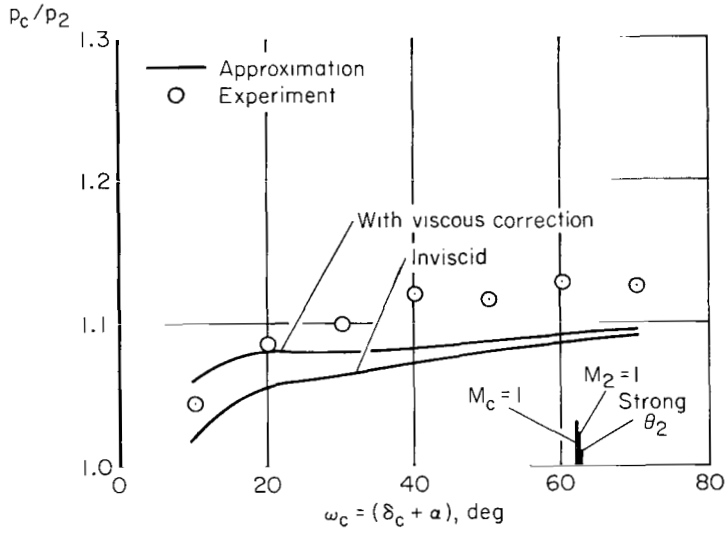

(b) $a/b = 1.5$; $\delta_c = 10.3^o$

Figure 17.- Comparison of approximate pressure ratio with experimental values for elliptical cones; $M_\infty = 10$, $\gamma = 1.4$, reference 14.

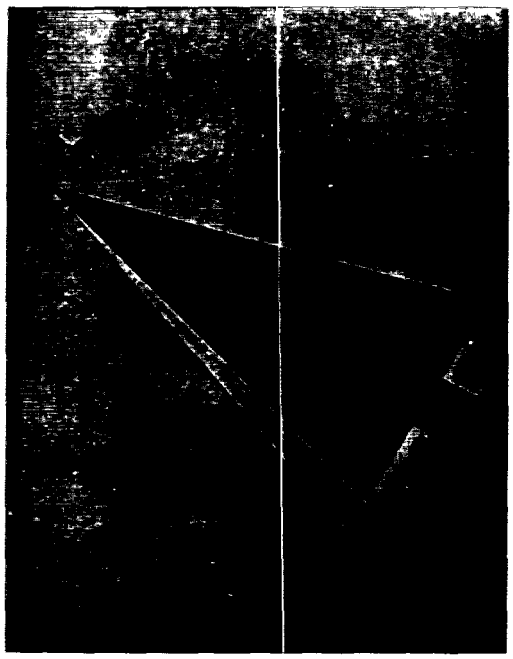

(a) $\alpha = 30^{\circ}$; $\omega_c = 45^{\circ}$
($M_2 \approx 1$)

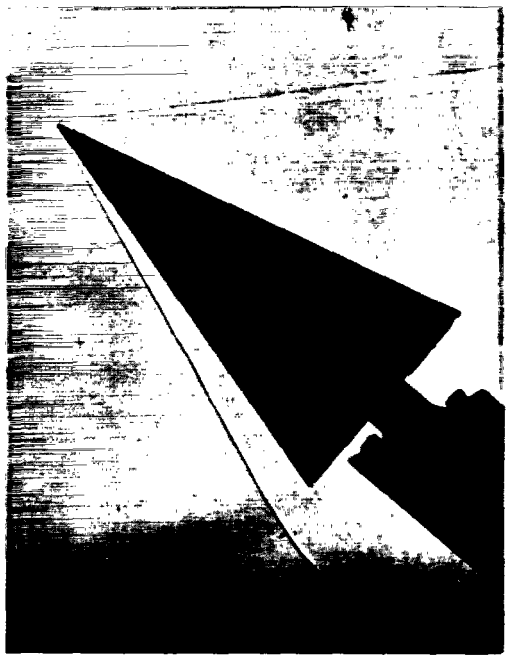

(b) $\alpha = 40^{\circ}$; $\omega_c = 55^{\circ}$
($M_2 < 1$)

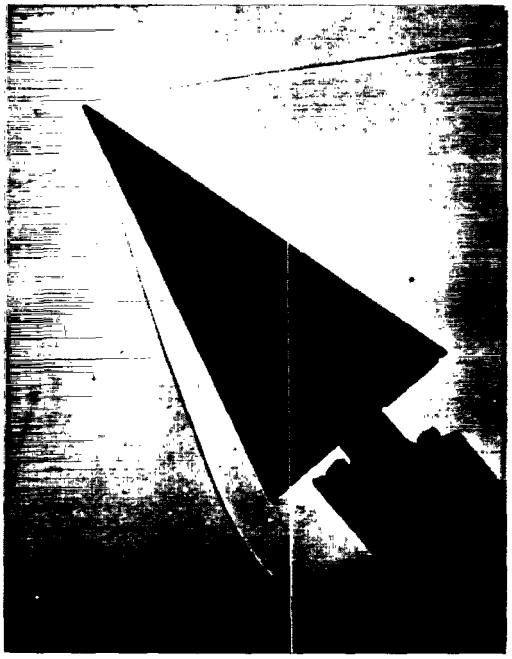

(c) $\alpha = 50^{\circ}$; $\omega_c = 65^{\circ}$
($M_2 < 1$)

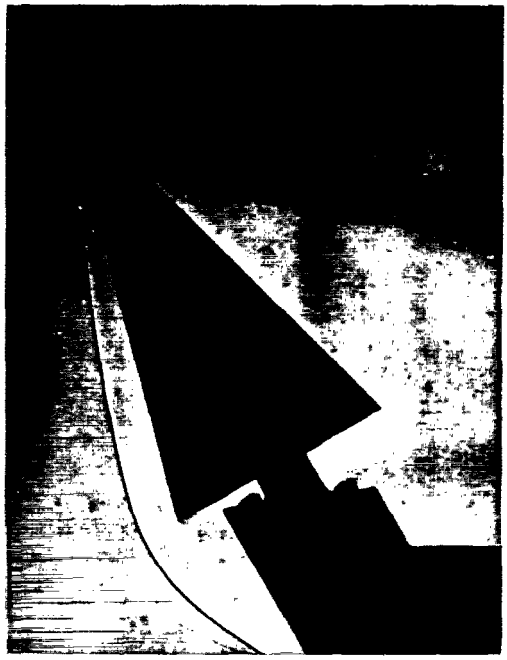

(d) $\alpha = 60^{\circ}$; $\omega_c = 75^{\circ}$
($M_2 < 1$)

Figure 18.- Shadowgraphs of the flow over a 15° semiapex cone; $M_\infty = 14.9$, $\gamma = 1.67$.

NASA-Langley, 1970 — 12 A-3615

"The aeronautical and space activities of the United States shall be conducted so as to contribute . . . to the expansion of human knowledge of phenomena in the atmosphere and space. The Administration shall provide for the widest practicable and appropriate dissemination of information concerning its activities and the results thereof."

—NATIONAL AERONAUTICS AND SPACE ACT OF 1958

NASA SCIENTIFIC AND TECHNICAL PUBLICATIONS

TECHNICAL REPORTS: Scientific and technical information considered important, complete, and a lasting contribution to existing knowledge.

TECHNICAL NOTES: Information less broad in scope but nevertheless of importance as a contribution to existing knowledge.

TECHNICAL MEMORANDUMS: Information receiving limited distribution because of preliminary data, security classification, or other reasons.

CONTRACTOR REPORTS: Scientific and technical information generated under a NASA contract or grant and considered an important contribution to existing knowledge.

TECHNICAL TRANSLATIONS: Information published in a foreign language considered to merit NASA distribution in English.

SPECIAL PUBLICATIONS: Information derived from or of value to NASA activities. Publications include conference proceedings, monographs, data compilations, handbooks, sourcebooks, and special bibliographies.

TECHNOLOGY UTILIZATION PUBLICATIONS: Information on technology used by NASA that may be of particular interest in commercial and other non-aerospace applications. Publications include Tech Briefs, Technology Utilization Reports and Notes, and Technology Surveys.

Details on the availability of these publications may be obtained from:

SCIENTIFIC AND TECHNICAL INFORMATION DIVISION

NATIONAL AERONAUTICS AND SPACE ADMINISTRATION

Washington, D.C. 20546